ACS APPLIED MATERIALS & INTERFACES

Letter

www.acsami.org

Highly Transparent and UV-Resistant Superhydrophobic SiO_2-Coated ZnO Nanorod Arrays

Yangqin Gao,[†] Issam Gereige,[†] Abdulrahman El Labban,[†] Dongkyu Cha,[‡] Tayirjan T. Isimjan,*[,†] and Pierre M. Beaujuge*[,†]

[†]Physical Sciences and Engineering Division and [‡]Advanced Nanofabrication, Imaging & Characterization Laboratory, King Abdullah University of Science and Technology (KAUST), Thuwal 23955-6900, Saudi Arabia

Supporting Information

ABSTRACT: Highly transparent and UV-resistant superhydrophobic arrays of SiO_2-coated ZnO nanorods are prepared in a sequence of low-temperature (<150 °C) steps on both glass and thin sheets of PET (2 × 2 in.^{2}), and the superhydrophobic nanocomposite is shown to have minimal impact on solar cell device performance under AM1.5G illumination. Flexible plastics can serve as front cell and backing materials in the manufacture of flexible displays and solar cells.

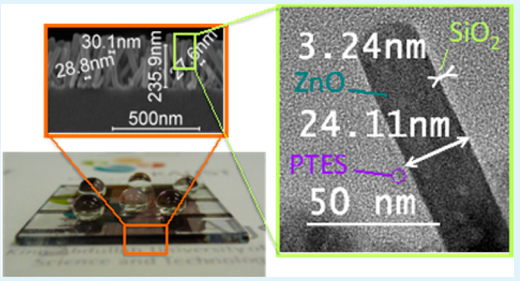

KEYWORDS: *transparent, superhydrophobic, ZnO nanorods, flexible coating, solar cell, nanocrystal arrays*

INTRODUCTION

Superhydrophobic coatings can have a significant impact on the development of glass and plastics with self-cleaning[1−4] and anti-fogging[5,6] properties, while also adding value to a wide range of tribological[7−9] and microfluidics applications.[10−13] In superhydrophobic coatings, hierarchical roughness introduces multiscale voids and gaps, trapping air at the material-water interface and, in turn, inducing high contact angles (>150°) with water droplets, low contact angle hysteresis and sliding angles.

The design and development of self-cleaning coatings for use in solar panels is especially important given that nearly half of the overall power conversion efficiency of solar panels can be lost due to dust accumulation every year.[14] In addition to the water- and dust-repellent property requirements, superhydrophobic coatings for photovoltaics must be highly transmissive to both visible and near-IR light as well as being UV-resistant and durable. A few recent studies discuss transparent superhydrophobic coatings applied to photovoltaics.[3,15,16] One promising approach utilizes solution-processed SiO_2-coated polymer microbeads that can be made hollow by calcination of the polymer template (350°C).[15] The resulting microcapsules can be bridged in a chemical vapor deposition (CVD) step with SiO_2 precursors to yield a mechanically resistant and highly transparent coating that can be applied to organic photovoltaic (OPV) devices on glass.[15] Meanwhile, approaches by which highly transmissive and nanostructured coating materials can be produced in a sequence of low-temperature steps (<150 °C) would make them applicable to a variety of flexible plastics, which is one of the key directions of research in the OPV community.[17]

Nanostructured oxides such as ZnO and TiO_2 possess high band gaps of ∼3.2 eV[18] and, as a result, high visible transmissivities, and can be either solution-processed[19−22] or hydrothermally grown using established methods.[23,24] Notably, as light scatters across oxide arrays, parasitic reflectivity is suppressed, such that nanostructured oxides can be used to improve the transparency of glass.[25−28] Here, we describe the preparation of a highly transmissive (avg. 93-95%) and UV-resistant superhydrophobic coating based on SiO_2-coated ZnO nanorod arrays grown on ultrathin seed layer (∼5 nm), and demonstrate that the presence of the superhydrophobic nanocomposite does not significantly impact the figures of merit of OPV devices. We also show that the sequential steps used for the preparation of the SiO_2/ZnO nanocomposite can be reproduced on a thin transparent sheet (2 × 2 in.^{2}) of polyethylene terephthalate (PET), which retains its superhydrophobicity upon repeated bending, suggesting that the superhydrophobic nanocomposite can be applied to flexible photovoltaics and displays.

RESULTS AND DISCUSSION

As part of the ZnO nanorod hydrothermal growth process, a seed layer of ZnO must be deposited on pre-cleaned glass (Fig. 1a, step 1) to lower the activation barrier for crystal nucleation.[29] Here, the seed layer was deposited by magnetron sputtering (see experimental section in the Supporting Information), and the dependence of seeded-glass transmissivity on the thickness of seed layer was examined by UV−vis spectroscopy. Figure 1b shows that the substrate transmittance gradually decreases as the thickness of the seed

Received: December 2, 2013
Accepted: February 4, 2014
Published: February 4, 2014

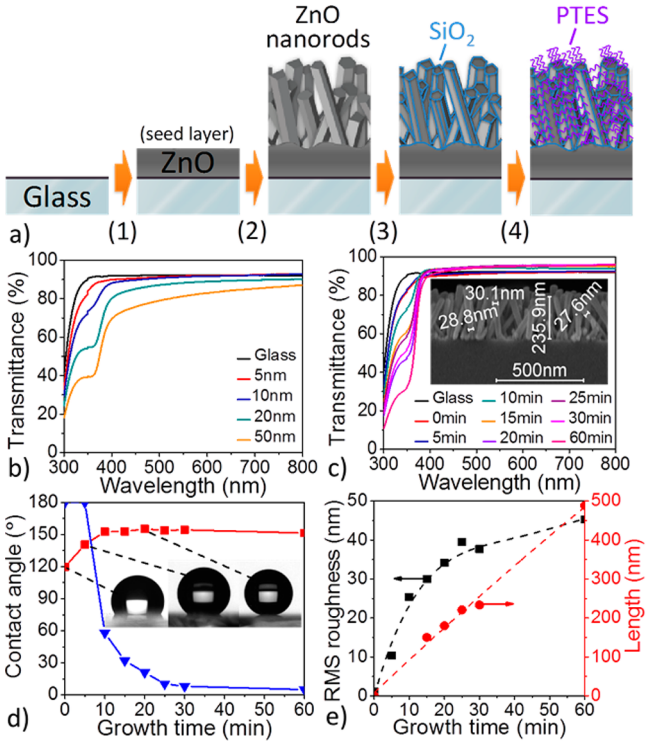

Figure 1. (a) Schematic description of the preparation of superhydrophobic SiO_2-coated ZnO nanorod arrays on glass (PTES = perfluorodecyltriethoxysilane). (b) Transmittance spectra of ZnO seed layers of various thicknesses (c) Transmittance spectra of ZnO nanorod arrays grown on 5 nm ZnO seed layer with different growth times. Inset: SEM cross-section of ZnO nanorods obtained after 25 min. (d) Evolution of the static (red square) and sliding (blue triangle) contact angles of PTES-treated ZnO nanorod arrays grown on 5 nm ZnO seed layer for various growth times. Inset: Photograph of a 2μL water droplet placed on selected PTES-treated ZnO nanorod arrays. (e) Evolution of the surface roughness (RMS) (black square) and average nanorod length (by SEM) (red circle) in relation to the ZnO-nanorod growth time.

layer increases, indicating that the seed layer should be as thin as possible in order to minimize both the parasitic absorption and reflection. With the refractive index of ZnO on the order of 2.0,[30] the reflection of incident light at the air−ZnO interface is expected to be greater than that at the air-glass interface. For example, in glass coated with a 50 nm seed layer (Figure 1b, orange curve), 10% (avg.) loss in transmittance is detected in the visible region (400−800 nm), while the transmittance drops by ca. 50% in the UV region, thus significantly reducing the number of photons transmitted to the active layer of any solar cell in this portion of the spectrum. In contrast, when the seed layer thickness approaches 5 nm (Figure 1b, red curve), the transmissivity of the ZnO-coated glass is nearly equivalent to that of glass alone across the full spectrum (300−800 nm), with a minimal transmittance loss near the band gap of ZnO. Meanwhile, the seed layer should be sufficiently stable, that is, thick enough, to allow effective and homogenous ZnO nanorod crystal growth by the hydrothermal approach.[31] Experimentally, we found that a thickness of a few nanometers is required. We thus set the seed layer thickness at 5 nm in all following steps.

To develop a superhydrophobic coating with the highest possible level of transparency, a trade-off between sufficient surface roughness and excessive scattering caused by overly long ZnO nanorods must be found. Figure 1c shows the evolution of the substrate transmittance as a function of the time allowed for crystal growth upon the seed layer (Figure 1a, step 2), and indicates a continuous loss of optical transmittance in the UV region as longer nanorods are formed. Interestingly, beyond 10 min of nanocrystal growth, the ZnO-coated glass substrate becomes more optically transmissive than bare glass in the visible region. This effect can be attributed to the graded transition of refractive index across the nanostructured coating acting as an anti-reflecting material at the interface between glass and air.[28,32] Meanwhile, as nanocrystal growth extends to 1h, the nanorod length reaches ∼500 nm on average (see Figure S1 in the Supporting Information), thus falling in the range of visible light wavelengths and resulting in significant parasitic scattering.[33] The higher degree of visible transparency is achieved after 25 min of nanocrystal growth (Figure S1 in the Supporting Information), as the nanorods reach a critical average length of ∼240 nm with their diameters on the order of 30 nm (Figure 1c, inset, and FigureS4 in the Supporting Information): transmissivity values in the 93-95% range, compared with 91−92% for uncoated glass. The X-ray diffraction (XRD) analysis of the corresponding nanostructured glass (see Figure S5 in the Supporting Information) shows a pronounced diffraction peak at $2\theta = 34.4°$ corresponding to the (001) crystal plane of ZnO and only a weak diffraction peak at $2\theta = 62.8°$ assignable to the (103) plane, indicating that most of the ZnO nanorods grow vertically on ZnO-seeded glass; this result is also shown qualitatively by scanning electron microscopy (SEM) (Figure 1c).

It is worth noting that the surface of as-prepared ZnO nanorod arrays is hydrophilic,[34] meaning that water droplets will rapidly wet ZnO-coated glass in spite of the significant roughness of the nanostructured oxide. Hydrophilic substrates exhibit small water contact angles and large sliding angles and, as such, they can easily accumulate water and dust. To circumvent the combined effect of polar hydroxyl groups at the ZnO surface and the capillary forces inducing the wettability, the nanorods are coated with a monolayer of perfluorodecyltriethoxysilane (PTES). At the ZnO nanorod surface, the PTES monolayer reduces the surface energy of the oxide,[35] and is expected to impart the superhydrophobicity. Figure 1d describes the superhydrophobic behavior of the perfluorinated ZnO nanorod arrays on glass as a function of the time allowed for crystal growth. While simple ZnO-seeded glass perfluorinated with PTES (t=0) shows low static contact angle values of 120°, static contact angles greater than 150° can be reached rapidly beyond 5 min of nanocrystal growth. Meanwhile, the ZnO-nanostructured glass remains dominated by large sliding angle values greater than 20° during the first 20 min of nanocrystal growth, and it is only after about 25 min that the nanorod arrays become truly superhydrophobic, with static contact angles greater than 150° (as high as 157°, Figure 1d inset) combined with markedly low sliding angles on the order of 10° and less (estimated from 2 μL water droplets). The influence of droplet size on sliding angle measurements is emphasized in Figure S2 in the Supporting Information. These results confirm that the surface state can be changed from Wenzel to Cassie−Baxter as the ZnO nanorods grow in length, that is, as the surface roughness increases as shown in Figure 1e. AFM images of a 5 nm ZnO seed layer sputtered on glass and the ZnO nanorod array after 25 min of growth are shown in Figure S3a and Figure S3b, respectively, in the Supporting Information. Here, we note that the aspect ratio of the AFM tip can be expected to limit the accuracy of the height profiles and

surface roughness (RMS) measurements performed on densely nanostructured surfaces such as the ones shown in Figure S3b in the Supporting Information, yet the relative comparison between RMS values (Figure 1e) remains reasonable. Considering both the high degree of transparency retained by the ~240 nm-long ZnO nanorod arrays obtained after 25 min of hydrothermal growth and their excellent superhydrophobic properties reached upon perfluorination with PTES, we used these arrays in the following steps and discussions.

While ZnO nanorods are typically prone to UV-triggered photo-oxidation reactions,[36,37] this shortcoming and the resulting gain in hydrophilicity can be circumvented by protecting the nanocrystal surface with a thin layer of UV-resistant material acting as a physical barrier.[23,24] Here, we chose to protect the ZnO surface by a thin layer of SiO_2 (Figure 1a, step 3) deposited by chemical vapor deposition (CVD) from tetraethoxysilane in the presence of ammonia (see experimental section in the Supporting Information).[15] The X-ray diffraction (XRD) pattern of the SiO_2-coated ZnO nanorods with varying SiO_2 deposition times (t = 0, 3, 6, 9, 12 h) is shown in Figure S5 in the Supporting Information, where the gradual reduction in the (001) diffraction peak intensity can be attributed to the screening of the ZnO nanorods by SiO_2. Figure 2a shows that layering SiO_2 on the ZnO nanorods does not further reduce the overall transmissivity of the nanostructured glass substrate. Thus, even after 6 h of SiO_2 deposition at an estimated growth rate of ca. 1 nm h^{-1}, the transmittance of the coating remains on the order of 45% (avg) in the UV region and on the order of 93−95% across the visible region; the thickness of the SiO_2 layer deposited after 3 and 6 h was determined by transmission electron microscopy (TEM) and the imaged SiO_2-coated ZnO nanorods are shown in Figure S6 in the Supporting Information, along with the energy-dispersive X-ray (EDX) analysis. As expected, the reflectance data shown in Figure S7 in the Supporting Information indicate that SiO_2-coated ZnO-nanostructured glass is less reflective (4−5%) than bare glass (8−9%). However, Figure S7 in the Supporting Information also indicates that the drop in the visible transmissivity of the SiO_2-coated ZnO nanorods beyond 6h of SiO_2 deposition (Figure 2a) can be correlated with an appreciable gain in the reflectance after the critical SiO_2 layer thickness is reached. This empirical observation is in agreement with the coarsening of the ZnO nanorod diameter upon SiO_2 deposition (Figure 2b) and with the corresponding reduction of RMS roughness as shown in Figure 2c upon SiO_2 deposition. The SEM cross-section of the SiO_2-coated ZnO nanorods shown in Figure S8 in the Supporting Information emphasizes the coarsening of the nanorod arrays resulting from 9 h of SiO_2 deposition. In such conditions, the nanorods are almost fully bridged by SiO_2, while a rather continuous top layer of oxide starts forming, which is expected to increase the overall reflectivity of the coating. Figure 2c confirms that, upon perfluorination of the SiO_2 layer with PTES (Figure 1a, step 4), the SiO_2-coated ZnO composite becomes superhydrophobic. While the static contact angle of ca. 157° remains fairly constant for SiO_2 layer thicknesses in the range 1-6 nm, the sliding angle reaches values as low as ca. 7° (~2−3 nm) and then increases gradually when the SiO_2 layer thicknesses surpass ~6 nm. With a sliding angle larger than 40° after 6 h of SiO_2 deposition (~7−8 nm), the superhydrophobicity of the nanostructured glass is compromised. This observation is consistent with the significant coarsening of the ZnO nanorod diameter upon SiO_2 deposition (Figure 2b).

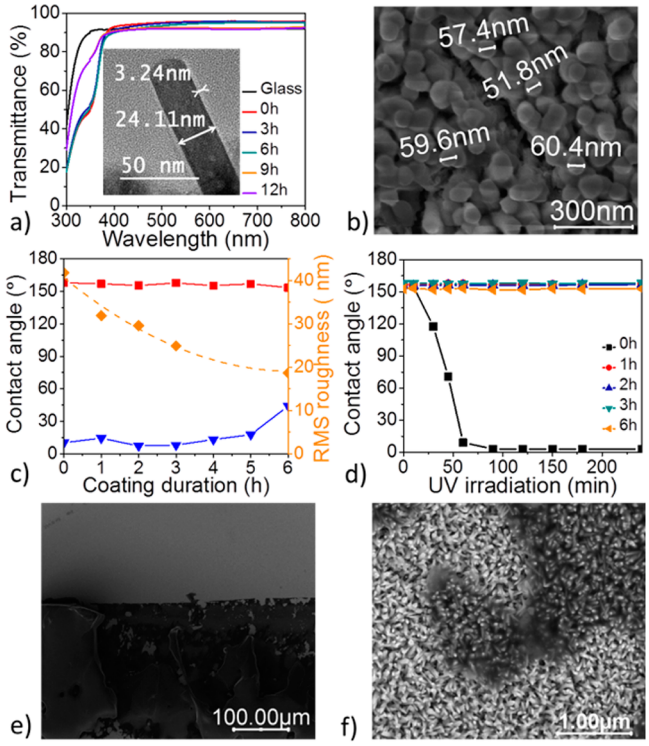

Figure 2. (a) Transmittance spectra of SiO_2-coated ZnO nanorods (grown for 25 min on a 5 nm ZnO seed layer) for various SiO_2 deposition times. Inset: TEM image of SiO_2-coated ZnO obtained after 3h of SiO_2 deposition. (b) SEM image (top-view) of the SiO_2-coated ZnO obtained after 6 h of SiO_2 deposition. (c) Evolution of contact angles and surface roughness (RMS) in PTES-treated SiO_2-coated ZnO nanorod arrays (grown for 25 min on 5 nm ZnO seed layer) for various SiO_2 deposition times: static contact angle (red square), sliding angle (blue triangle), surface roughness (yellow diamond). (d) Evolution of contact angles on PTES-treated SiO_2-coated ZnO nanorod arrays with UV irradiation time (365 nm, ~2 mW cm^{-2}) (e) SEM image of the SiO_2/ZnO nanocomposite surface after application and subsequent removal of a scotch tape pressed at 10 kPa for 1 min: the adhesive (dark region) peels off and remains bound to the nanostructured coating. (f) Magnified SEM image showing that the integrity of the nanorod arrays is retained under the bound adhesive (darker regions).

Importantly, Figure 2d shows that thin SiO_2 layers of ca. 1 nm (1h deposition) are sufficient to protect the ZnO nanorod surface and to avoid the dramatic increase in hydrophilicity caused by UV-triggered photo-oxidation reactions. In parallel, the robustness of the SiO_2-coated ZnO nanorod arrays on glass was qualitatively assessed with a "scotch tape" experiment in which the adhesive tape was pressed at 10 kPa against the nanostructured surface for 1 min (see details in the Supporting Information). Figure 2e shows that, upon removing the tape, the adhesive peels off from the backing material and remains bound to the SiO_2-coated ZnO nanorod arrays. The magnification of the nanostructured coating under the bound adhesive shown in Figure 2f confirms that the integrity of the nanorod arrays is retained.

To demonstrate the minimal impact of the presence of the superhydrophobic nanorod arrays on solar cell performance, we prepared bulk-heterojunction (BHJ) devices with the polymer donor PBDTTPD[38−40] and the fullerene acceptor $PC_{71}BM$ (see device fabrication in the Supporting Information). The configuration of the OPV device including the SiO_2/ZnO

dx.doi.org/10.1021/am405513k | ACS Appl. Mater. Interfaces 2014, 6, 2219−2223

nanocomposite is shown in Figure 3a; Figure 3b shows perfectly spherical droplets positioned on the front of the

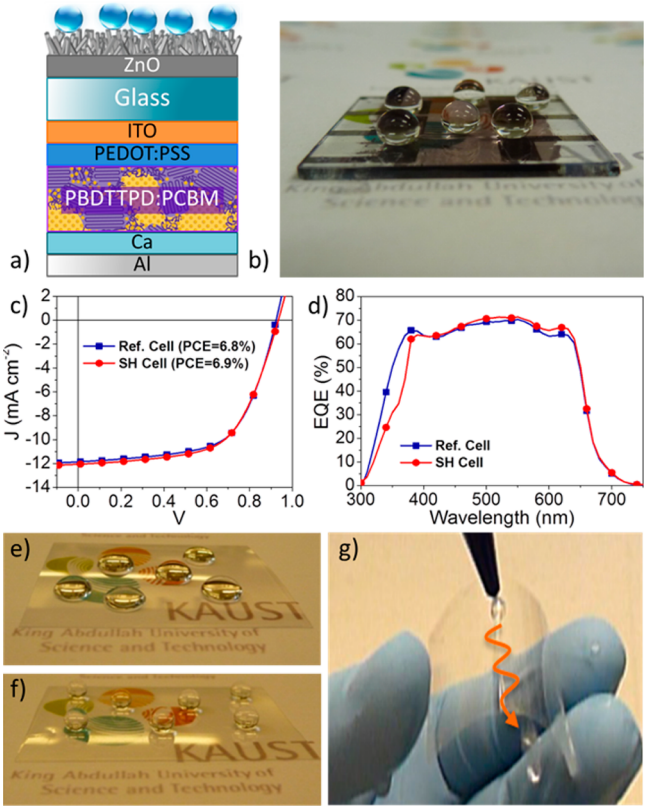

Figure 3. (a) Schematic of a BHJ polymer solar cell including the SiO2/ZnO nanocomposite. (b) Water droplets positioned on the front of the superhydrophobic device remain perfectly spherical. (c) *J*–*V* characteristic of a superhydrophobic (SH) cell (red circle) superimposed on that of a bare reference (Ref.) cell (blue square); AM1.5G solar illumination (100 mW cm^{-2}). (d) EQE spectra of the SH cell (red circle) and the Ref. cell (blue square). (e) Water droplets positioned on a bare transparent sheet of PET (2 × 2 $in.^2$). (f) Droplets positioned on superhydrophobic PET (static angle: 160°). (g) PET retains its superhydrophobicity upon repeated bending (×350) (extracted from Video S1in the Supporting Information).

superhydrophobic device (static angle, 157°; sliding angle, 13°). The superhydrophobic cell (red curve, circles) and bare reference cell (blue curve, squares) under AM1.5G solar illumination (100 mW cm^{-2}) (Figure 3c) exhibit equivalent *J*–*V* characteristics with comparable power conversion efficiencies (PCEs) of 6.9 and 6.8%, respectively, values comparable within the limits of experimental accuracy. In parallel, their external quantum efficiency (EQE) spectra (Figure 3d) show comparably broad and efficient EQE responses, with values >60% in the 370–630 nm range, and peaking at ca. 70% at 550 nm, which confirms the minimal impact of the presence of the superhydrophobic nanorod arrays on solar cell performance.

Ultimately, approaches to the preparation of highly transmissive superhydrophobic coatings in a sequence of low-temperature (<150 °C) steps may be applicable to a variety of flexible plastics, which can serve as front cell and backing materials in the manufacture of flexible displays and solar cells. Noting that ZnO nanorod arrays can be grown hydrothermally on various plastics such as polyethylene terephthalate (PET),[41] polydimethylsiloxane (PDMS),[42] and polyimide,[43] we considered reproducing the sequential steps used for the preparation of our SiO_2-coated ZnO superhydrophobic coating on a thin transparent sheet of PET (2 × 2 $in.^2$). Under the same experimental protocol (see experimental section in the Supporting Information), the PET surface, initially hydrophobic (Figure 3e), became superhydrophobic while retaining its high visible transmissivity (Figure 3f). On PET, the excellent static contact angle of 160°, comparable to that obtained earlier on glass (157°), was found to be relatively invariant upon repeated bending (Figure 3g; ×350), a promising result in the context of future flexible thin-film device applications.

CONCLUSION

In summary, we have described the preparation of a highly transmissive (avg. 93–95%) and UV-resistant superhydrophobic coating based on SiO_2-coated ZnO nanorod arrays. On the one hand, we showed that the highest degree of coating transparency can be achieved upon carefully optimizing (i) the seed layer thickness and (ii) the size of the ZnO nanorods. On the other hand, we emphasize the critical dependence of the superhydrophobicity on (i) the ZnO nanorod length, (ii) the thickness of the SiO_2 layer and (iii) the presence of a UV-protective layer (here SiO_2, only a few nm suffice) for the ZnO nanorods. The superhydrophobic SiO_2/ZnO nanocomposite has minimal impact on solar cell device performance under AM1.5G illumination, and the sequential steps used for its preparation are applicable to both glass and plastics, thus validating the suggestion that the superhydrophobic arrays can be utilized in flexible displays and solar cells.

ASSOCIATED CONTENT

Supporting Information

Experimental and characterization methods; enlarged transmittance spectra for ZnO nanorod arrays with different growth times; influence of droplet size on sliding angle; AFM and cross-section SEM image of ZnO nanorods with 25 min growth time; XRD, TEM, EDX, and reflectance spectra of SiO_2-coated ZnO nanorods; top-view and cross-section SEM image of ZnO nanorods with SiO_2 deposition time of 3 and 9 h. Video S1 demonstrates retained superhydrophobicity after repeated bending of superhydropbic coated PET. This material is available free of charge via the Internet at http://pubs.acs.org.

AUTHOR INFORMATION

Corresponding Author

*E-mail: pierre.beaujuge@kaust.edu.sa.

Notes

The authors declare no competing financial interest.

ACKNOWLEDGMENTS

The authors acknowledge the financial support of the Office of Competitive Research Funds (OCRF) at King Abdullah University of Science and Technology (KAUST) under the "Competitive Research Grant" (CRG) program No. FIC/2010/02. The authors thank the Advanced Imaging and Characterization Laboratories at KAUST for technical support. Y.G. thanks Prof. Boon Ooi and Dr. TienKhee Ng for helpful discussions and useful scientific insights. The authors thank Dr. Clément Cabanetos for providing the PBDTTPD polymer.

REFERENCES

(1) Kota, A. K.; Li, Y. X.; Mabry, J. M.; Tuteja, A. Hierarchically Structured Superoleophobic Surfaces with Ultralow Contact Angle Hysteresis. *Adv. Mater.* **2012**, *24*, 5838−5843.

(2) Bhushan, B.; Jung, Y. C.; Koch, K. Self-Cleaning Efficiency of Artificial Superhydrophobic Surfaces. *Langmuir* **2009**, *25*, 3240−3248.

(3) Zhu, J.; Hsu, C. M.; Yu, Z. F.; Fan, S. H.; Cui, Y. Nanodome Solar Cells with Efficient Light Management and Self-Cleaning. *Nano Lett.* **2010**, *10*, 1979−1984.

(4) Nishimoto, S.; Bhushan, B. Bioinspired Self-Cleaning Surfaces with Superhydrophobicity, Superoleophobicity, and Superhydrophilicity. *RSC Adv.* **2013**, *3*, 671−690.

(5) Chen, Y.; Zhang, Y. B.; Shi, L.; Li, J.; Xin, Y.; Yang, T. T.; Guo, Z. G. Transparent Superhydrophobic/Superhydrophilic Coatings for Self-Cleaning and Anti-Fogging. *Appl. Phys. Lett.* **2012**, *101*, 033701.

(6) Lai, Y. K.; Tang, Y. X.; Gong, J. J.; Gong, D. G.; Chi, L. F.; Lin, C. J.; Chen, Z. Transparent Superhydrophobic/Superhydrophilic TiO_2-Based Coatings for Self-Cleaning and Anti-Fogging. *J. Mater. Chem.* **2012**, *22*, 7420−7426.

(7) Mertaniemi, H.; Jokinen, V.; Sainiemi, L.; Franssila, S.; Marmur, A.; Ikkala, O.; Ras, R. H. A. Superhydrophobic Tracks for Low-Friction, Guided Transport of Water Droplets. *Adv. Mater.* **2011**, *23*, 2911−2914.

(8) Shirtcliffe, N. J.; McHale, G.; Newton, M. I.; Zhang, Y. Superhydrophobic Copper Tubes with Possible Flow Enhancement and Drag Reduction. *ACS Appl. Mater. Interfaces* **2009**, *1*, 1316−1323.

(9) Jin, H.; Kettunen, M.; Laiho, A.; Pynnonen, H.; Paltakari, J.; Marmur, A.; Ikkala, O.; Ras, R. H. A. Superhydrophobic and Superoleophobic Nanocellulose Aerogel Membranes as Bioinspired Cargo Carriers on Water and Oil. *Langmuir* **2011**, *27*, 1930−1934.

(10) Zahner, D.; Abagat, J.; Svec, F.; Frechet, J. M. J.; Levkin, P. A. A Facile Approach to Superhydrophilic-Superhydrophobic Patterns in Porous Polymer Films. *Adv. Mater.* **2011**, *23*, 3030−3034.

(11) Mumm, F.; van Helvoort, A. T. J.; Sikorski, P. Easy Route to Superhydrophobic Copper-Based Wire-Guided Droplet Microfluidic Systems. *ACS Nano* **2009**, *3*, 2647−2652.

(12) Yao, X.; Song, Y. L.; Jiang, L. Applications of Bio-Inspired Special Wettable Surfaces. *Adv. Mater.* **2011**, *23*, 719−734.

(13) You, I.; Kang, S. M.; Lee, S.; Cho, Y. O.; Kim, J. B.; Lee, S. B.; Nam, Y. S.; Lee, H. Polydopamine Microfluidic System toward a Two-Dimensional, Gravity-Driven Mixing Device. *Angew. Chem. Int. Ed.* **2012**, *51*, 6126−6130.

(14) Elminir, H. K.; Ghitas, A. E.; Hamid, R. H.; El-Hussairly, F.; Beheary, M. M.; Abdel-Moneim, K. M. Effect of Dust on the Transparent Cover of Solar Collectors. *Energy Convers. Manage.* **2006**, *47*, 3192−3203.

(15) Deng, X.; Mammen, L.; Zhao, Y. F.; Lellig, P.; Mullen, K.; Li, C.; Butt, H. J.; Vollmer, D. Transparent, Thermally Stable and Mechanically Robust Superhydrophobic Surfaces Made from Porous Silica Capsules. *Adv. Mater.* **2011**, *23*, 2962−2965.

(16) Park, Y. B.; Im, H.; Im, M.; Choi, Y. K. Self-Cleaning Effect of Highly Water-Repellent Microshell Structures for Solar Cell Applications. *J. Mater. Chem.* **2011**, *21*, 633−636.

(17) Arias, A. C.; MacKenzie, J. D.; McCulloch, I.; Rivnay, J.; Salleo, A. Materials and Applications for Large Area Electronics: Solution-Based Approaches. *Chem. Rev.* **2010**, *110*, 3−24.

(18) Wei, B.; Zheng, K.; Ji, Y.; Zhang, Y.; Zhang, Z.; Han, X. Size-Dependent Bandgap Modulation of ZnO Nanowires by Tensile Strain. *Nano Lett.* **2012**, *12*, 4595−9.

(19) Ebert, D.; Bhushan, B. Transparent, Superhydrophobic, and Wear-Resistant Coatings on Glass and Polymer Substrates Using SiO_2, ZnO, and ITO Nanoparticles. *Langmuir* **2012**, *28*, 11391−11399.

(20) Zhang, X.; Kono, H.; Liu, Z.; Nishimoto, S.; Tryk, D. A.; Murakami, T.; Sakai, H.; Abe, M.; Fujishima, A. A Transparent and Photo-Patternable Superhydrophobic Film. *Chem. Commun.* **2007**, 4949−4951.

(21) Kim, J. H.; Lee, M.; Lim, T. Y.; Hwang, J. H.; Kim, E.; Kim, S. H. Fabrication of Transparent Superhydrophobic ZnO Thin Films by a Wet Process. *J. Ceram. Process. Res.* **2010**, *11*, 259−262.

(22) Tarwal, N. L.; Patil, P. S. Superhydrophobic and Transparent ZnO Thin Films Synthesized by Spray Pyrolysis Technique. *Appl. Surf. Sci.* **2010**, *256*, 7451−7456.

(23) Wang, L. L.; Zhang, X. T.; Fu, Y.; Li, B.; Liu, Y. C. Bioinspired Preparation of Ultrathin SiO_2 Shell on ZnO Nanowire Array for Ultraviolet-Durable Superhydrophobicity. *Langmuir* **2009**, *25*, 13619−13624.

(24) Xue, C. H.; Yin, W.; Jia, S. T.; Ma, J. Z. UV-Durable Superhydrophobic Textiles with UV-Shielding Properties by Coating Fibers with ZnO/SiO_2 Core/Shell Particles. *Nanotechnology* **2011**, *22*, 415603.

(25) Kwak, G.; Jung, S.; Yong, K. Multifunctional Transparent ZnO Nanorod Films. *Nanotechnology* **2011**, *22*, 115705.

(26) Lee, Y. J.; Ruby, D. S.; Peters, D. W.; McKenzie, B. B.; Hsu, J. W. P. ZnO Nanostructures as Efficient Antireflection Layers in Solar Cells. *Nano Lett.* **2008**, *8*, 1501−1505.

(27) Clapham, P. B.; Hutley, M. C. Reduction of Lens Reflection by the "Moth Eye" Principle. *Nature* **1973**, *244*, 281−282.

(28) Raguin, D. H.; Morris, G. M. Antireflection Structured Surfaces for the Infrared Spectral Region. *Appl. Opt.* **1993**, *32*, 1154−1167.

(29) Sugunan, A.; Warad, H. C.; Boman, M.; Dutta, J. Zinc Oxide Nanowires in Chemical Bath on Seeded Substrates: Role of Hexamine. *J. Sol−Gel Sci. Technol.* **2006**, *39*, 49−56.

(30) Yoshikawa, H.; Adachi, S. Optical Constants of ZnO. *Jpn. J. Appl. Phys., Part 1* **1997**, *36*, 6237−6243.

(31) Liu, J.; She, J. C.; Deng, S. Z.; Chen, J.; Xu, N. S. Ultrathin Seed-Layer for Tuning Density of ZnO Nanowire Arrays and Their Field Emission Characteristics. *J. Phys. Chem. C* **2008**, *112*, 11685−11690.

(32) Enger, R. C.; Case, S. K. Optical Elements with Ultrahigh Spatial-Frequency Surface Corrugations. *Appl. Opt.* **1983**, *22*, 3220−3228.

(33) Karunakaran, R. G.; Lu, C. H.; Zhang, Z. H.; Yang, S. Highly Transparent Superhydrophobic Surfaces from the Coassembly of Nanoparticles (≤100 nm). *Langmuir* **2011**, *27*, 4594−4602.

(34) Kwak, G.; Seol, M.; Tak, Y.; Yong, K. Superhydrophobic ZnO Nanowire Surface: Chemical Modification and Effects of UV Irradiation. *J. Phys. Chem. C* **2009**, *113*, 12085−12089.

(35) Nishino, T.; Meguro, M.; Nakamae, K.; Matsushita, M.; Ueda, Y. The Lowest Surface Free Energy Based on -CF_3 Alignment. *Langmuir* **1999**, *15*, 4321−4323.

(36) Qin, H. C.; Li, W. Y.; Xia, Y. J.; He, T. Photocatalytic Activity of Heterostructures Based on ZnO and N-Doped ZnO. *ACS Appl. Mater. Interfaces* **2011**, *3*, 3152−3156.

(37) Tian, Z. R. R.; Voigt, J. A.; Liu, J.; McKenzie, B.; McDermott, M. J.; Rodriguez, M. A.; Konishi, H.; Xu, H. F. Complex and Oriented ZnO Nanostructures. *Nat. Mater.* **2003**, *2*, 821−826.

(38) Beaujuge, P. M.; Frechet, J. M. J. Molecular Design and Ordering Effects in π-Functional Materials for Transistor and Solar Cell Applications. *J. Am. Chem. Soc.* **2011**, *133*, 20009−20029.

(39) Cabanetos, C.; El Labban, A.; Bartelt, J. A.; Douglas, J. D.; Mateker, W. R.; Frechet, J. M. J.; McGehee, M. D.; Beaujuge, P. M. Linear Side Chains in Benzo[1,2-*b*:4,5-*b*′]dithiophene-Thieno[3,4-*c*]pyrrole-4,6-dione Polymers Direct Self-Assembly and Solar Cell Performance. *J. Am. Chem. Soc.* **2013**, *135*, 4656−4659.

(40) Piliego, C.; Holcombe, T. W.; Douglas, J. D.; Woo, C. H.; Beaujuge, P. M.; Frechet, J. M. J. Synthetic Control of Structural Order in *N*-Alkylthieno[3,4-*c*]pyrrole-4,6-dione-Based Polymers for Efficient Solar Cells. *J. Am. Chem. Soc.* **2010**, *132*, 7595−7597.

(41) Lee, Y. J.; Sounart, T. L.; Scrymgeour, D. A.; Voigt, J. A.; Hsu, J. W. P. Control of ZnO Nanorod Array Alignment Synthesized via Seeded Solution Growth. *J. Cryst. Growth* **2007**, *304*, 80−85.

(42) Kim, M. K.; Yi, D. K.; Paik, U. Tunable, Flexible Antireflection Layer of ZnO Nanowires Embedded in PDMS. *Langmuir* **2010**, *26*, 7552−7554.

(43) Ahn, H.; Park, J. H.; Kim, S. B.; Jee, S. H.; Yoon, Y. S.; Kim, D. J. Vertically Aligned ZnO Nanorod Sensor on Flexible Substrate for Ethanol Gas Monitoring. *Electrochem. Solid-State Lett.* **2010**, *13*, J125−J128.